

VELOCITY FIELDS AS A TRACER FOR MAGNETIC FIELDS IN SUB-ALFVÉNIC REGIMES: THE VELOCITY GRADIENT TECHNIQUE

DIEGO F. GONZÁLEZ-CASANOVA AND A. LAZARIAN

Astronomy Department, University of Wisconsin-Madison, 475 North Charter Street, Madison, WI 53706-1582, USA

Draft version April 15, 2022

ABSTRACT

Strong Alfvénic turbulence develops eddy-like motions perpendicular to the local direction of magnetic fields. This local alignment induces velocity gradients perpendicular to the local direction of the magnetic field. We use this fact to propose a new technique of studying the direction of magnetic fields from observations, the Velocity Gradient Technique. We test our idea by employing the synthetic observations obtained via 3D MHD numerical simulations for different sonic and Alfvén Mach numbers. We calculate the velocity gradient, Ω , using the velocity centroids. We find that Ω traces the projected magnetic field best for the synthetic maps obtained with sub-Alfvénic simulations providing good point-wise correspondence between the magnetic field direction and that of Ω . The reported alignment is much better than the alignment between the density gradients and the magnetic field and we demonstrated that it can be used to find the magnetic field strength using the Chandrasekhar-Fermi method. Our study opens a new way of studying magnetic fields using spectroscopic data.

Subject headings: ISM: magnetic fields, kinematics and dynamics - magnetohydrodynamics (MHD) - turbulence

1. INTRODUCTION

It is well established that the interstellar medium (ISM) is turbulent, affecting the dynamics of different astrophysical phenomena such as star formation, cosmic ray acceleration, galaxy evolution, and feedback (Ferrière 2001; Elmegreen & Scalo 2004; de Avillez & Breitschwerdt 2005; McKee & Ostriker 2007; Falgarone et al. 2008). Widely-used evidence of the turbulence in the ISM is seen in the so-called Big Power Law in the Sky (Armstrong et al. 1995; Chepurnov & Lazarian 2010) that reflects the Kolmogorov spectrum of electron density fluctuations, in nonthermal Doppler broadening (see Draine 2011), in the power-law scalings of the fluctuations measured in Position-Position Velocity (PPV) space (see Lazarian & Pogosyan 2000; Stanimirović & Lazarian 2001; Chepurnov et al. 2010, 2015; Padoan et al. 2009) (see Lazarian et al. 2009, for a review), and in velocity centroids (see Miesch et al. 1999; Miville-Deschênes et al. 2003).

Detection and measurement of magnetic fields present a challenging problem. Polarization arising from grains aligned with longer axes perpendicular to a magnetic field allows for estimation of the direction of the magnetic field, but the uncertainties in grain alignment and failure of grain alignment at large optical depths limit the ability of the technique to trace magnetic fields without ambiguities (see Lazarian 2007; Lazarian et al. 2015, for a review). This affects the Chandrasekhar-Fermi technique that is being used to find the intensity of magnetic fields when the variations of dust alignment are known together with the measurements of the velocity dispersion. The Zeeman effect, Goldreich-Kylafis effect have their own limitations (see Crutcher 2012). Faraday rotation can measure the intensity of the field along the line of sight (Padoan et al. 2001; Ostriker 2003; Crutcher

2012). Therefore there is intense interest in developing new techniques. For instance, the anisotropy analysis of statistical properties (Lazarian et al. 2002; Esquivel & Lazarian 2005; Heyer & Brunt 2004; Esquivel & Lazarian 2009; Burkhart et al. 2015) proved to be a promising way of obtaining the mean magnetic field as well as the media magnetization. Atomic alignment is another technique that can be used, but its work has not been demonstrated yet (see Yan & Lazarian 2012, for a review). The difference of the velocities of ions and neutrals due to the difference of their damping in MHD turbulence has been suggested as another way of studying magnetic fields. The technique has its limitations, however (see Xu et al. 2015). All in all, the search of new ways of studying magnetic fields is characterized by intensive research with all techniques having their shortcomings and limitations. In the present paper we propose a new technique of magnetic field study, the Velocity Gradient Technique (VGT).

The Chandrasekhar & Fermi (1953, C-F) method can determine magnetic field strengths by estimating the small-scale randomness of the magnetic field lines, assuming Alfvénic motions (Ostriker et al. 2001; Houde et al. 2009; Novak et al. 2009). The C-F method estimates the magnetic field strength as:

$$B \approx \sqrt{4\pi\rho} \, \delta v / \delta\phi, \quad (1)$$

where ρ is the density, δv is the velocity dispersion, and $\delta\phi$ is the polarization angle dispersion. Two-point correlation analysis in the form of structure functions on the polarization dispersion has been used to enhance the ability to determine the direction of the magnetic field and thus better constrains the magnetic field than the classical C-F method (Falceta-Gonçalves et al. 2008). Furthermore, this method can determine the intensity of the magnetic field with less than a 20% uncertainty. Cho &

Yoo (2016) show that velocity dispersion, measured with velocity centroids, is independent of the turbulence injection scale, and hence a more accurate C-F method.

In a strongly magnetized turbulent medium, the turbulent eddies determine the properties of the turbulence, such as energy dissipation and time scales. The eddies also have a preferential direction of motion, set by the local direction of the magnetic field (Goldreich & Sridhar 1995). This leads to an energy cascade that depends on the direction of the magnetic field (Cho et al. 2002a). Since eddies represent the dynamics of the turbulence and have a preferential axis of rotation, an analysis on their rotation would determine the direction of the magnetic field. Moreover, since eddies are rotating at different velocities determined by the medium, there is a velocity gradient along the medium that is perpendicular to the rotation axis.

In this *paper* we present a new technique, the VGT, to measure the direction of the magnetic field using velocity gradients. The velocity gradient is obtained from velocity centroids and utilizes the turbulent eddies that are stretched along the magnetic field to trace the interstellar magnetic field. In Section 2, we explore the theoretical approach to the use of velocity gradients; in Section 3, we describe the numerical code and setup for the simulations; in Section 4, we present our method of the VGT and the alignment with the magnetic field; in Section 5, we present different properties of the velocity gradients; in Section 6, we discuss our technique; and in Section 7, we give our conclusions.

2. THEORETICAL CONSIDERATIONS

In weak Alfvénic turbulence the Alfvénic waves dominate the motion of the medium (with their wave vector in the direction of the magnetic field). In strong MHD turbulence, for both sub- and super- Alfvénic regimes the turbulence motion type is eddy-like, just like in the hydrodynamical case. Goldreich & Sridhar (1995), henceforth GS95, developed the theory of strong MHD turbulence dominated by eddy motions that develop an energy cascade. However, unlike the hydrodynamical case, the eddy motions have a preferential direction of motion set by the magnetic field direction (Montgomery & Turner 1981; Shebalin et al. 1983; Higdon 1984). Since the magnetic field direction in larger eddies defines the direction of anisotropy for smaller eddies (local direction of the magnetic field), is important to understand of the local system of reference at each eddy in order to identify its properties. This analysis is done with a wavelet description (see Kowal & Lazarian 2010).

The local system of reference is one of the major pillars of the modern understanding of MHD turbulence (Lazarian & Vishniac 1999; Cho & Vishniac 2000; Maron & Goldreich 2001; Cho et al. 2002b). In this local frame, the scales of the eddies are set by a “critical balance”:¹

$$l_{\parallel}^{-1} V_A \approx l_{\perp}^{-1} u_l, \quad (2)$$

with V_A the Alfvén speed, u_l the eddy velocity, and l_{\parallel} and l_{\perp} the eddy scales parallel and perpendicular to the local direction of the magnetic field. The Alfvén speed

V_A is: $\langle |\mathbf{B}| \rangle / \sqrt{\langle \rho \rangle}$, where $\langle \cdot \rangle$ is the average over the entire data set. This critical condition determines the eddy size by the distance an Alfvénic perturbation can propagate during an eddy turnover (for a review see Lazarian et al. 2012). For the sub-Alfvénic regime the eddy velocity and scales can be written in terms of the injection velocity (V_L) as (Lazarian & Vishniac 1999):

$$\begin{aligned} l_{\parallel} &\approx L \left(\frac{l_{\perp}}{L} \right)^{2/3} M_A^{-4/3}, \\ u_l &\approx V_L \left(\frac{l_{\perp}}{L} \right)^{1/3} M_A^{1/3}, \end{aligned} \quad (3)$$

where $M_A = \langle |\mathbf{v}| / V_A \rangle$ is the Alfvénic Mach number, $|\mathbf{v}|$ is the local magnitude of the velocity field, and L is the injection scale with injection velocity V_L . These intrinsic properties of the eddies imprinted by the Alfvénic turbulence imply not only the condition of a preferential direction along the local magnetic field, but also that the eddy velocity depends the size of the eddy. The effects of the anisotropy of the velocity fluctuations on the turbulent medium have been described by analyzing intensity anisotropies of Position Position Velocity (PPV) channels (Lazarian & Pogosyan 2000; Burkhart et al. 2014; Esquivel et al. 2015; Kandel et al. 2016b), correlations of velocity centroids (Esquivel & Lazarian 2005; Federath et al. 2010; Kandel et al. 2016a), the bispectrum (Burkhart et al. 2009), and higher order statistical moments (Kowal et al. 2007), as well as using Principal Component Analysis (PCA) (Heyer et al. 2008).

The local system of reference cannot be studied in observations where the averaging along the line of sight is performed. The projection effects inevitably mask the actual direction of the magnetic field within individual eddies along the line of sight. As a result, the scale-dependent anisotropy predicted in the Goldreich & Sridhar (1995) model is not valid for the observer measuring parallel and perpendicular scales of projected and averaged (along the line of sight) eddies. The anisotropy of eddies becomes scale-independent and the degree of anisotropy gets determined by the anisotropy of the largest eddies for which projections are mapped (Cho & Lazarian 2002a; Esquivel & Lazarian 2005). The projections of eddies for sub-Alfvénic turbulence is aligned along the magnetic field.

The elongated eddies have the largest velocity gradient perpendicular to the their longest axes. Thus we expect the direction of the maximum velocity gradient to be perpendicular to the local magnetic field. In the case of sub-Alfvénic turbulence, the local and global directions of the magnetic field are aligned. Thus, the velocity gradients can map-trace the directions of the magnetic field.

3. MHD SIMULATIONS

We used two MHD codes to simulate the data, AMUN for the sub-Alfvénic regime (Kowal et al. 2007, 2009) and a code developed by Cho & Lazarian (2002b) for the super-Alfvénic regime. Both codes solve the ideal MHD equations with periodic boundary conditions,

¹ The original GS95 treated the motions in the frame of the mean field.

$$\begin{aligned}
\frac{\partial \rho}{\partial t} + \nabla \cdot (\rho \mathbf{v}) &= 0, \\
\frac{\partial \rho \mathbf{v}}{\partial t} + \nabla \cdot \left[\rho \mathbf{v} \mathbf{v} + \left(p + \frac{B^2}{8\pi} \right) \mathbf{I} - \frac{\mathbf{B} \mathbf{B}}{4\pi} \right] &= \mathbf{f}, \\
\frac{\partial \mathbf{B}}{\partial t} &= \nabla \times (\mathbf{v} \times \mathbf{B}), \\
p &= c_s^2 \rho, \\
\nabla \cdot \mathbf{B} &= 0,
\end{aligned} \tag{4}$$

were ρ is the density, p is the pressure, c_s is the isothermal sound speed, \mathbf{B} is the magnetic field, \mathbf{v} is the velocity and is \mathbf{f} the external force (in this case the turbulence injection force).

The turbulence is driven solenoidally in Fourier space at a scale 2.5 times smaller than the simulation box size, i.e. $2.5 l_{inj} = l_{box}$. This scale defines the injection scale in our modes in Fourier space. Density structures in turbulence can be associated with the effects of slow and fast modes (Beresnyak et al. 2005; Kowal et al. 2007). The code units of length are defined in terms of the box size (L), and the time as the eddy turnover time (L/v). For this simulation the velocity and density fields are set to unity in code units while the pressure was changed to get the different sonic Mach numbers. The simulations are isothermal scale-free, so they can be scaled for any parameters of the observed media studied (see Burkhart et al. 2009) provided that the cooling in the media is efficient to keep it isothermal. The properties of different phases of the interstellar medium can be found at Draine & Lazarian (1998).

The magnetic field has a uniform component (\mathbf{B}_0) and a fluctuating field ($\delta \mathbf{b}$), i.e. ($\mathbf{B} = \mathbf{B}_0 + \delta \mathbf{b}$). Initially $\delta \mathbf{b} = 0$ and for all times $\langle \delta \mathbf{b} \rangle = 0$. The fluctuating field is produced due to the turbulence injection. The mean field is in the ‘ x ’ direction. The database consists of 5 numerical simulations with a resolution of 256^3 for the super-Alfvénic and 192^3 for the sub-Alfvénic regime, where the mean magnetic field has values of 10, 1, and 0.1 (see Table 1), where the values of the magnetic field are given in the units of velocity driving. Therefore magnetic field $B=10$ corresponds to the Alfvén Mach number $M_A = V_L/V_A = 0.1$, where V_L is the velocity at the scale L of turbulent injection. The supersonic simulations have a resolution of 512^3 . For most of the analysis we use the first 3 models.

4. ALIGNMENT OF VELOCITY GRADIENTS AND MAGNETIC FIELD

4.1. Velocity centroids

Observational information, such as velocity, density, intensity and magnetic field, correspond to the projected information of the 3D medium. The projection is done along the line of sight (LOS) generating a 2D field known as the plane of the sky.

One of the frequently used techniques to obtain velocity spectra using spectral lines is based on the analysis of velocity centroids, which are first moments of spectral line (see Münch & Wheelon 1958; Kleiner & Dickman 1985; O’dell & Castaneda 1987; Miesch et al. 1999). Velocity centroids were also suggested as a means of mea-

TABLE 1
SIMULATION PARAMETERS

Model	\mathbf{B}_0	M_A	M_S	σ^S	m^S	θ_χ^S	σ^C	m^C	Resolution
1	10	0.11	0.7	24°	81°	77°	23°	81°	192 ³
2	1	0.74	0.7	26°	78°	74°	26°	78°	256 ³
3	0.1	2.77	0.7	47°	53°	56°	48°	53°	256 ³
4	1	0.74	2	34°	70°		33°	71°	512 ³
5	1	0.74	7	45°	56°		43°	61°	512 ³
6	0.1	2.77	2	50°	48°		50°	48°	512 ³

suring anisotropy of turbulence using velocity correlations (Esquivel & Lazarian 2005, 2009; Burkhart et al. 2014). A theoretical elaboration of the latter technique using the analytical description of PPV (Lazarian & Pogosyan 2000, 2004, 2008) was obtained in Kandel et al. (2016a).

Velocity centroids $C(\mathbf{x})$ and $S(\mathbf{x})$ (normalized and un-normalized respectively),² give information on the velocity field of the medium. Apart from velocity centroids we use intensity of total emission. For our model we assume that the intensity, $I(\mathbf{x})$, is proportional to the column density, just like the case of optically thin HI emission:

$$\begin{aligned}
C(\mathbf{x}) &= \frac{\int v_z(\mathbf{x}, z) \rho(\mathbf{x}, z) dz}{\int \rho(\mathbf{x}, z) dz}, \\
S(\mathbf{x}) &= \int v_z(\mathbf{x}, z) \rho(\mathbf{x}, z) dz, \\
I(\mathbf{x}) &= \int \rho(\mathbf{x}, z) dz,
\end{aligned} \tag{5}$$

where ρ is the density, v_z is the LOS component of the velocity, \mathbf{x} is the position of the plane of the sky, and ‘ z ’ is the position along the LOS. Using equation 5 we construct three 2D maps with the mean magnetic field, \mathbf{B}_0 , perpendicular to the LOS. One map for the intensity (density) and two for the centroids (velocity).

While velocities directly trace turbulence, density is a much more distorted tracer, especially at high Mach numbers (Beresnyak et al. 2005; Kowal et al. 2007). Thus we do not expect the gradients of column densities to trace magnetic fields well.

We compare the directions of projected velocity centroid gradients with the direction of projected magnetic fields. The magnetic fields were also projected along the LOS by:

$$\mathbf{B}_x(\mathbf{x}) = \int \mathbf{B}_x(\mathbf{x}, z) dz, \tag{6}$$

$$\mathbf{B}_y(\mathbf{x}) = \int \mathbf{B}_y(\mathbf{x}, z) dz, \tag{7}$$

where \mathbf{B}_x and \mathbf{B}_y are the components of the magnetic field perpendicular to the LOS. The map of the projected magnetic field is shown in Figures 1 and 2.

4.2. The velocity gradient technique

² The traditionally-used centroids are normalized, but the study in Esquivel & Lazarian (2005) showed that for practical purposes, the normalization does not give much, but significantly complicates the study. Thus we introduced un-normalized centroids which were used for many subsequent studies (see Kandel et al. 2016a).

The velocity gradient present in the local system of the 3D eddies, is projected onto the plane of the sky using the velocity centroids. Hence, the velocity gradient has to be estimated in two dimensions and is affected by projection effects. The maximum gradient, ∇ , is defined as:

$$\nabla^U(\mathbf{x}) = \max \left\{ \frac{|U(\mathbf{x}) - U(\mathbf{x} + \mathbf{x}')|}{|\mathbf{x}'|} \right\}, \quad (8)$$

where $U(\mathbf{x})$ is the projected information ($C(\mathbf{x})$ or $S(\mathbf{x})$), and \mathbf{x}' is defined in a circular punctured neighborhood around the point \mathbf{x} of radius r . For our calculations we use $r = 10$. To estimate the lag effects on the velocity gradient we modify the lag for the estimation of the velocity gradient, ranging from 2 to 64, in powers of 2^n . The results are independent of the lag for lags larger than ~ 8 . Below this size the circular neighborhood presents the effects of a square grid, slightly increasing the error on the measurement. The velocity gradient field, $\Omega(\mathbf{x})$, that marks the direction of the maximum gradient is defined as:

$$\Omega^U(\mathbf{x}) = \mathbf{x}' . \quad (9)$$

Ω is therefore constructed such that its direction is preferentially perpendicular to the local magnetic field. Figure 1 shows the projected magnetic field and the rotated 90° velocity gradient vector. The rotation is used to account for the fact that the velocity gradients are expected to be perpendicular to the magnetic field, as we discussed above. We observe a fair alignment of magnetic field and the rotated velocity gradients obtained with velocity centroids.

To compare the alignment between two vector fields – in this case Ω and \mathbf{B} – one can use the angle between the two vectors. Two different angle measurements were used. One measures the full angle span (0° – 180°), giving information on the actual magnetic field vector (ϕ). The second measures the relative direction of the vectors constructing the magnetic field pseudo-vectors (θ). Hence, the *pseudo-angle* will only be measured between 0° and 90° (0° implying a parallel configuration and 90° a perpendicular one). Figure 2 shows the magnetic field (\mathbf{B}), gradient field for the un-normalized centroid (Ω^S), and the angle and pseudo-angle between the two fields for the three models (ϕ^S and θ^S). We can observe that the correlation of magnetic field direction and the gradient direction is the best for high degrees of media magnetization, i.e. corresponding to $B = 10$ and gets worse for super-Alfvénic turbulence with $B = 0.1$. We remind our reader that the magnetization that was used in our earlier papers (see Esquivel & Lazarian 2005; Burkhart et al. 2014; Esquivel et al. 2015) was measured with Alfvén Mach number M_A which is $\sim 1/B$ for the units adopted in this paper and the exact values can be found in table 1.

Figure 3 shows the cumulative pseudo-angle distribution for the different models, and the distribution for the un-normalized centroid. The normalized (C) and un-normalized centroids (S) give a similar angle distribution. Table 1 gives the standard deviation, σ , for the angle distribution and the median, m , for the pseudo-angle distribution for both C and S . $90^\circ - m$ can be in-

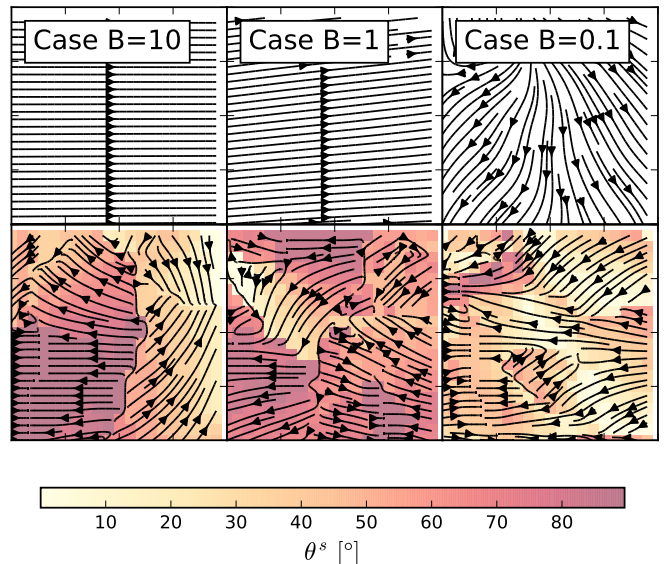


FIG. 1.— *Top row:* projected magnetic field, \mathbf{B} . *Bottom row:* gradient field for the un-normalized centroids, Ω^S rotated 90° , so it is *parallel* to the magnetic field and the angle between the magnetic field and the gradient. All plots correspond to a subregion of 20 cells of the simulation. Therefore, the maps do not represent the overall performance of the technique, for that see the cumulative distribution in Figure 3.

terpreted as the error in the distribution at which half of the sample is perpendicular to the magnetic field. Since C and S have similar angles distributions, future analysis will center on the un-normalized centroid (section 5). This figure quantitatively illustrates the correlation of the magnetic field with the velocity gradients measured by centroids, as well as the variation of this correlation with the media magnetization.

The different panels of Figure 3 present the results using different styles. For instance, the upper panel shows in a histogram or probability distribution that in most cases for $B = 10$ the velocity gradients tend to be aligned perpendicular to the plane-of-sky magnetic field. The lower panels present the information in their cumulative distribution that presents information not in counts but rather in its “percentile”. The percentile indicates the value below which a given percentage of observations in a group of observation fall. For example the 50th percentile is the same as the median, at which point half of the observations are below that observation (Zwillinger & Kokoska 1999). The black line corresponds to no correlation and the deviations from these line are proportional to the alignment of the magnetic field. The larger the deviation the better the alignment, as a higher percentage of the data is closer to 90° . All panels show that, for instance, the correlation for $B = 0.1$ is marginal, as it is, in fact, expected for super-Alfvénic turbulence for which the GS95 scalings are not applicable for large scales of motions.

4.3. Alignment of density gradients and magnetic fields

The velocity gradient technique traces the intrinsic velocity gradient present in a turbulent medium. The turbulence also has its imprint on the density distribution. Hence, one can do an analysis, similar to the one used on the velocity centroids, to the density (intensity), $I(\mathbf{x})$. As shown in figure 3, the density gradient is not that well

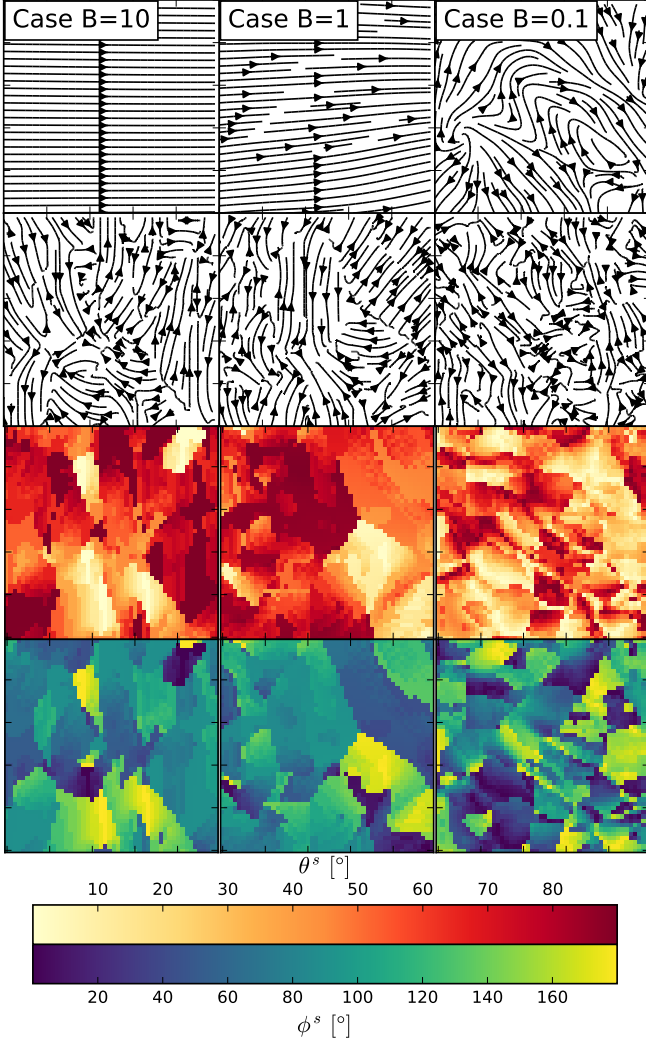


FIG. 2.— *Top row*: projected magnetic field, \mathbf{B} . *Middle-top row*: gradient field for the un-normalized centroids, Ω^S . *Middle-bottom row*: pseudo-angle between the two vector fields, θ^S , with its 180° ambiguity, and *Bottom row*: angle between the two vector fields, ϕ^S . From left to right the different models decrease the magnetic field strength. All plots correspond to a subregion of 50 cells of the simulation. The figure presents how the technique of the velocity gradient looks on a subsection of the simulation.

correlated with the direction of the magnetic field, giving much larger error estimates for the direction of the magnetic field.

Soler et al. (2013) suggested that the density gradients are correlated with the direction of the magnetic field. The gradient is calculated using the square neighborhood around the cell. In Figure 3, we present the correlation of *column density gradients* with the magnetic field. Our analysis shows that the velocity gradients give a more accurate direction of the magnetic field. The problematic nature of using density gradients is expected to increase for high Mach number turbulence when the density fluctuations lose clear correlation with magnetic field, e.g. low contrast density fluctuations may be parallel to magnetic field as in GS95 picture (Beresnyak et al. 2005), which large contrast may be perpendicular or not well aligned.

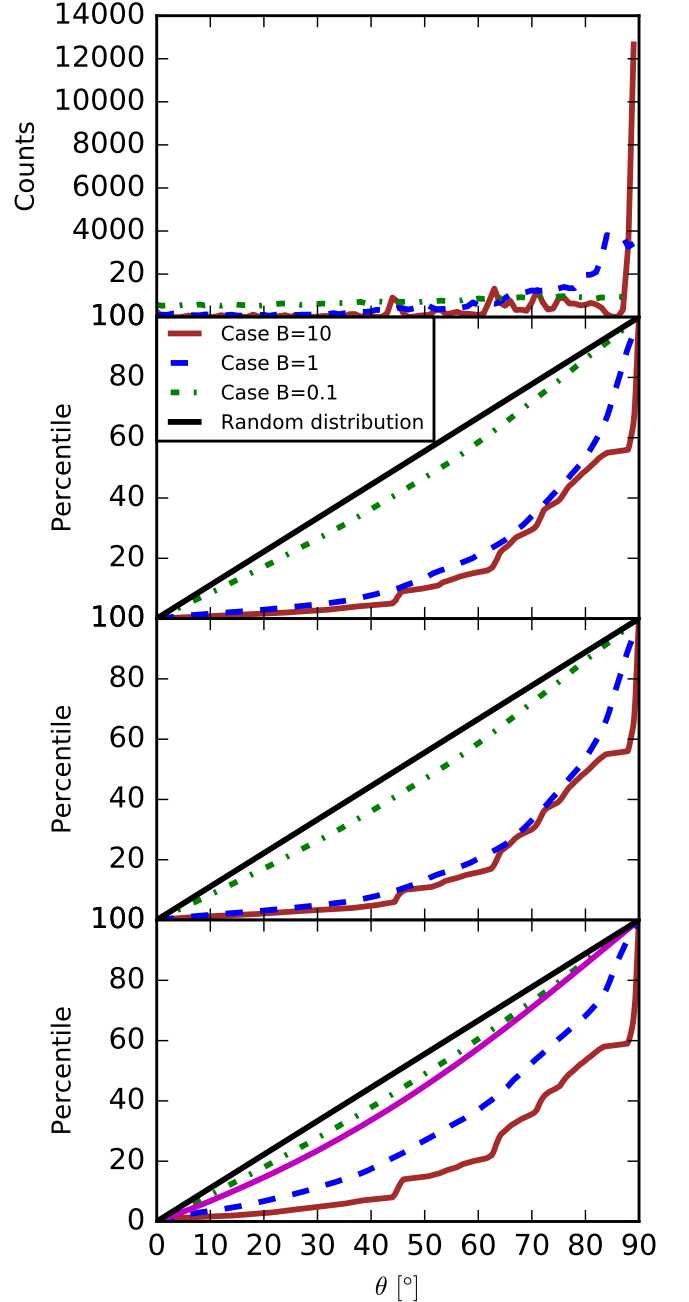


FIG. 3.— Cumulative pseudo-angle distribution for the three magnetic field intensities and the distribution for the un-normalized centroid (S ; *Top panel*). *Middle-top panel* for the normalized centroid (C). *Middle-bottom panel* for the un-normalized centroid (S). *Bottom panel* for the intensity (I). In *magenta* is the angle distribution of the gradient technique developed by Soler et al. (2013) corresponding to $M_A \approx 3.1$ with a kernel of 3×3 . Soler et al. (2013) use the technique in self-gravity clouds and they measure the full angle between the gradient and the magnetic field. For this plot we fold the the distribution to a pseudo-angle distribution.

5. IMPLICATIONS OF THE MAGNETIC FIELD ALIGNMENT WITH GRADIENTS

5.1. χ^2 test

It is known that the local system of reference of the eddies cannot be studied with observational information, since the projection masks the direction of the local alignment of the magnetic field and the eddies. This local

projected alignment between the velocity gradient and the magnetic field gives rise to a more complex alignment distribution than just a perpendicular one (Figure 3). Given this complex distribution one can estimate the most common angle by means of a reduced Pearson χ^2 test:

$$\chi^2 = \frac{1}{N} \sum_{i=1}^N \frac{(O_i - E_i)^2}{E_i}, \quad (10)$$

where N is the number of data points, O_i is the observed angle, and E_i is the estimated angle that reduces the χ^2 test. Figure 4 shows χ^2 for all cases assuming pseudo-angle distribution. The χ^2 for the full angle distribution peaks at 90° independently of the level of magnetization. The values of the angle that minimize the χ^2 test, θ_χ^S , are in Table 1. This test was used because it is the simplest tool that explores the parameter space, in this case the alignment between the projected magnetic field and velocity, and determines the most likely parameter, in this case θ_χ^S .

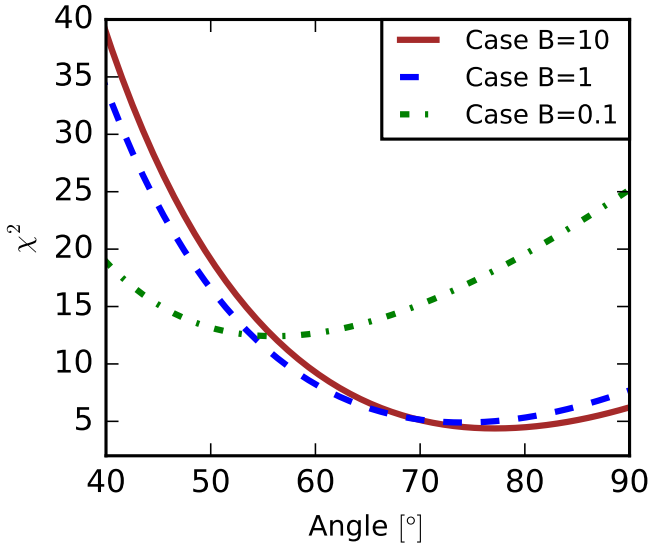


FIG. 4.— The reduced χ^2 test was used to analyze the parameter space of alignment between the projected magnetic field and velocity centroids. χ^2 is plotted as a function of angle of the three magnetic field intensities for the un-normalized centroid. Where the χ^2 minimize is the most likely angle distribution between the two projected quantities.

5.2. Anisotropy

Correlation functions are a two-point statistical tool. In a turbulent medium they can be used to measure the power spectrum of the energy cascade, and to analyze the anisotropy of the medium (Esquivel et al. 2003; Esquivel & Lazarian 2005):

$$CF(\mathbf{r}) = \left\langle f(\mathbf{x}) \cdot f(\mathbf{x} + \mathbf{r}) \right\rangle, \quad (11)$$

where CF is the correlation function, \mathbf{r} is the “lag”, $\langle \cdot \rangle$ denotes the average over all points, and f denotes the desired function – in this case the velocity centroids, intensity and velocity gradient. The power and energy spec-

trum can be estimated by a correlation function of the velocity centroid.

The anisotropies of the medium are measured using the correlation functions by making the lag a function of the angle to the global mean magnetic field, $\mathbf{r}(\theta)$. The angle θ has a span of 90° , going from $\mathbf{r}(0^\circ) = \mathbf{r}_\parallel$ ($\mathbf{r}_\parallel \times \mathbf{B} = 0$) to $\mathbf{r}(90^\circ) = \mathbf{r}_\perp$ ($\mathbf{r}_\perp \cdot \mathbf{B} = 0$). In an isotropic medium the values of the correlation function should be independent of the direction of the lag, i.e. $CF(\mathbf{r}_\parallel) = CF(\mathbf{r}_\perp)$. In the case of an anisotropic medium, such as in Alfvénic turbulence, the correlation presents a preferential direction. The preferential direction is set by the mean magnetic field – in other words, the correlation function changes depending on the direction of the mean magnetic field. The intensity of the magnetic field determines the level of the anisotropy and hence the elongation of the isocontours of the velocity centroids (Figure 5). The mean direction of the magnetic field sets the elongation direction of the isocontours.

Applying the same method of correlation functions to the velocity gradient $\boldsymbol{\Omega}$, one can see that just as the velocity centroid is affected by the intensity of the magnetic field, so is the velocity gradient. Hence, the correlation function of the velocity gradient can determine the level of magnetization of the medium and the direction of the mean field to determine if the velocity gradient technique can be used.

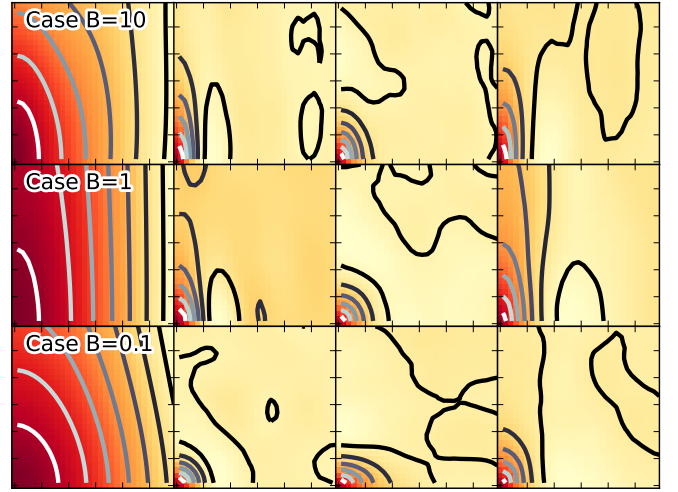


FIG. 5.— Correlation function as a function of angle with respect to the mean magnetic field for all cases. From left to right: S , $|\Omega_x^S|$, and $|\Omega_y^S|$. From top to bottom the mean magnetic field intensities: 10, 1, and 0.1.

5.3. Statistical moments of the velocity gradient

The different levels of magnetization produced in the medium modify the distribution of the velocity gradient, $\boldsymbol{\Omega}$. These differences on the distribution are quantized by the statistical moments. We use the L-moments to understand its properties and relate them to the Alfvénic mach number. L-moments, introduced by Hosking (1990), measure the properties of the distribution like regular statistical moments. The L-moments use are as defined in (Wang 1996) and the L-moment ratios are $t_3 = l_3/l_2$ and $t_4 = l_4/l_2$:

$$\begin{aligned}
l_1 &= \frac{1}{C_1^n} \sum_{i=1}^n x_i, \\
l_2 &= \frac{1}{2} \frac{1}{C_2^n} \sum_{i=1}^n (C_1^{i-1} - C_1^{n-1}) x_i, \\
l_3 &= \frac{1}{3} \frac{1}{C_3^n} \sum_{i=1}^n (C_2^{i-1} - 2C_1^{i-1}C_1^{n-1} - C_2^{n-1}) x_i, \\
l_4 &= \frac{1}{4} \frac{1}{C_4^n} \sum_{i=1}^n (C_3^{i-1} - 3C_2^{i-1}C_1^{n-1} + 3C_1^{i-1}C_2^{n-1} - C_3^{n-1}) x_i,
\end{aligned}$$

where x_i is the data sample, and C_m^n is the number of combination of m items from n defined as:

$$C_k^m = \frac{m!}{k!(m-k)!}. \quad (12)$$

Because L-moments are a linear function of the data, they are less susceptible to sampling variability (such as outliers in the data) than conventional moments. The L-moment ratios such as L-skew (t_3) and L-kurtosis (t_4) have the property $|t_i| < 1$.

The two components of the velocity gradient (parallel and perpendicular to the mean magnetic field) and the magnitude of the gradient are analyzed separately using the L-moments for the full angle span (0° to 180°). Ω_x^S is the component of the velocity gradient that is parallel to the mean magnetic field while Ω_y^S is in the perpendicular direction. L-skew and L-mean are close to zero for all the cases of the velocity gradient components, giving no information on the intensity of the magnetic field. The L-mean and L-skew for Ω_x^S is always constant (as a function of M_A) since its distribution always has a peak around 90° (perpendicular to the magnetic field), for Ω_y^S the lack of changes are due to no preferential direction of motion set by the magnetic field and therefore a more homogeneous medium. The L-kurtosis and L-mean are shown as a function of the Alfvénic mach number in Figure 6. The moments are only a function of M_A for Ω_x^S since it is the component susceptible to the changes in the intensity of the field. The decrease in the L-kurtosis and increase in the L-scale for Ω_x^S reflects that Ω^S is mostly perpendicular to the magnetic field with most of its components around zero. This implies that given a distribution of the velocity gradient, measuring the L-moments for both components one can estimate the intensity of the magnetic field and its global direction. To estimate the mean field direction it is necessary that the components of the velocity gradient match those presented here.

5.4. Chandrasekhar-Fermi method

The C-F method has been used to determine the intensity of the magnetic field on the plane of the sky using the velocity and polarization measurements. Here we use the properties of the velocity gradient and velocity to determine the intensity of the field, modifying the original C-F method. Equation 1 is rewritten in terms of the velocity centroid for the velocity dispersion, and the angle dispersion from the velocity gradient (σ^U). For the case of transonic turbulence and any degree of magnetization the C-F method can be rewritten as:

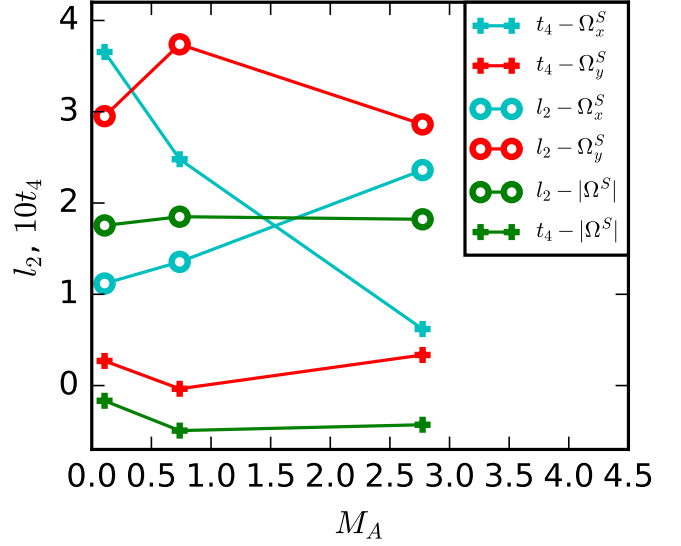


FIG. 6.— L-kurtosis (circles) and L-scale (crosses) for Ω_x^S (cyan), Ω_y^S (red), and $|\Omega^S|$ (green) as a function of the Alfvénic mach number. The L-moments for Ω_x^S and Ω_y^S have the same trends.

$$B = \gamma \sqrt{4\pi\rho} \frac{\delta v}{\sigma^U}, \quad (13)$$

where γ for the intensity (I) is ~ 3 , and for both velocity centroids is ~ 2.95 . Now we can understand how this approximation changes with the sonic mach number. For this analysis we use all the data cubes (Table 1) to understand the properties of the sonic mach number (M_S) on the velocity gradient estimation and on the C-F analysis. Figure 7 shows the standard deviation and errors to the magnetic field intensity as a function of M_S . With the inclusion of the sonic data, the C-F transforms to:

$$B = \gamma \sqrt{4\pi\rho} \frac{\delta v}{\sigma^U - \beta}, \quad (14)$$

with β for the centroids and intensity ~ 0.31 , for the five models. As seen in Figure 7 the error estimates for the intensity are higher than those for the velocity centroids.

6. DISCUSSION

6.1. Smoothing effects

Data smoothing can be a source of error in the technique. In order to take into account the data smoothing, we use two different smoothing kernels on the velocity centroids – a square and a Gaussian kernel. For the square kernel, each point in the velocity centroid is replaced with the average of the points in its vicinity. In this case, the vicinity was defined as square boxes of lag $r = 2^n$ with n from 0 to 6. The velocity gradient is then estimated using the smooth velocity centroids and the un-smoothed magnetic field. This process reduces or increases the different values as seen in Table 2. The process of smoothing is thus not a technique to enhance the results in all cases.

The Gaussian smoothing kernel was used to simulate more realistic observational data. Namely, observational data does not have pencil-thin beam resolution, but more of a smooth beam resolution. We use 4 values for the full-width-half-maximum (FWHM) of 2, 4, 8 and 16. The

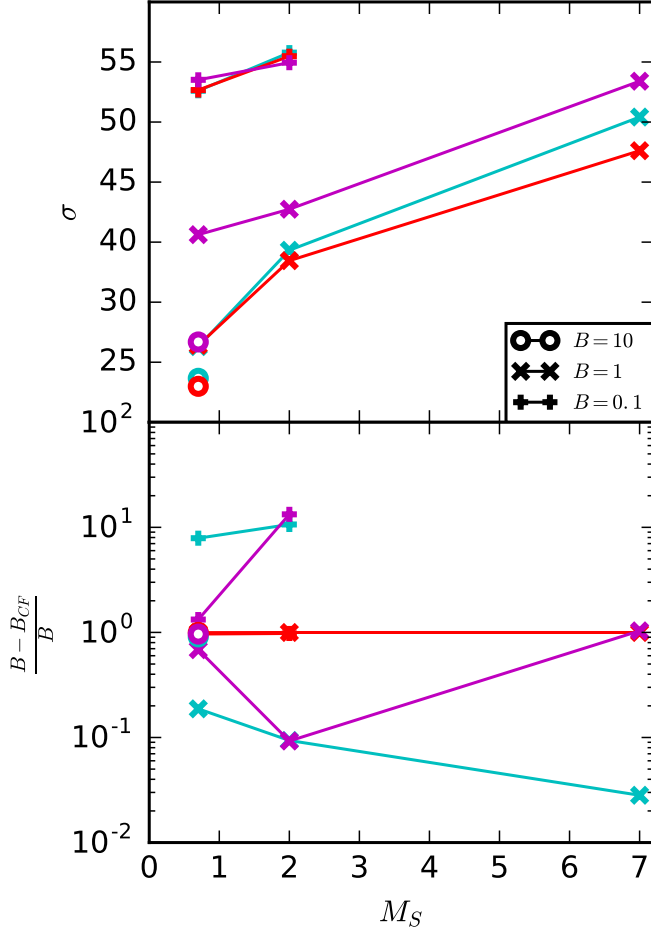


FIG. 7.— *Top panel:* The dispersion, measured with the standard deviation (σ), as a function of the sonic mach number (M_S) for the three different gradients. In *magenta*: σ^I , *incyan*: σ^S , and *red*: σ^C . A similar trend, but with smaller errors is found on the pseudo-angle distribution. *Bottom panel* the relative error estimation between the magnetic field (from the simulation) and the estimation from the C-F method as a function of M_S for the different magnetization levels.

TABLE 2
SMOOTHING EFFECTS OF THE SQUARE KERNEL

lag 'r'	Model B = 10			Model B = 1		
	σ^S	m^S	θ_χ^S	σ^S	m^S	θ_χ^S
0	24°	81°	77°	23°	81°	75°
2	26°	77°	75°	26°	78°	74°
4	30°	72°	72°	26°	78°	74°
8	34°	67°	68°	26°	79°	74°
16	35°	66°	67°	24°	81°	76°
32	33°	71°	70°	17°	81.5°	78°
64	32°	68°	70°	20°	81.5°	77°

process of Gaussian smoothing also increases the errors like square smoothing.

6.2. Column density effects

The effects of column density on the understanding of the structure of the magnetic field has been a point of discussion (Evans 1999; Clark et al. 2014; Koch & Rosolowsky 2015; Ntormousi et al. 2016; Planck Collaboration et al. 2016). To address this issue, the intensity

TABLE 3
SMOOTHING EFFECTS OF THE GAUSSIAN KERNEL

FWHM	Model B = 10		Model B = 1	
	σ^S	m^S	σ^S	m^S
0	24°	81°	26°	78°
2	29°	72°	28°	72°
4	35°	67°	35°	67°
8	40°	65°	40°	65°
16	41°	53°	41°	53°

(column density) maps for models 1 and 2 (Table 1), are divided into three equally-size intervals. Giving three column density intervals for each of the models (low, mid, and high). The gradient for the intensity and the unnormalized centroid as calculated in section 4, are filtered using the column density criterion. Using only the low and high column density data the cumulative distribution is obtained as shown in Figure 8. For both degrees of magnetization and both gradients, Ω^I and Ω^S , the low column density has smallest errors, followed by the global calculation, and then high column density ones (Table 4).

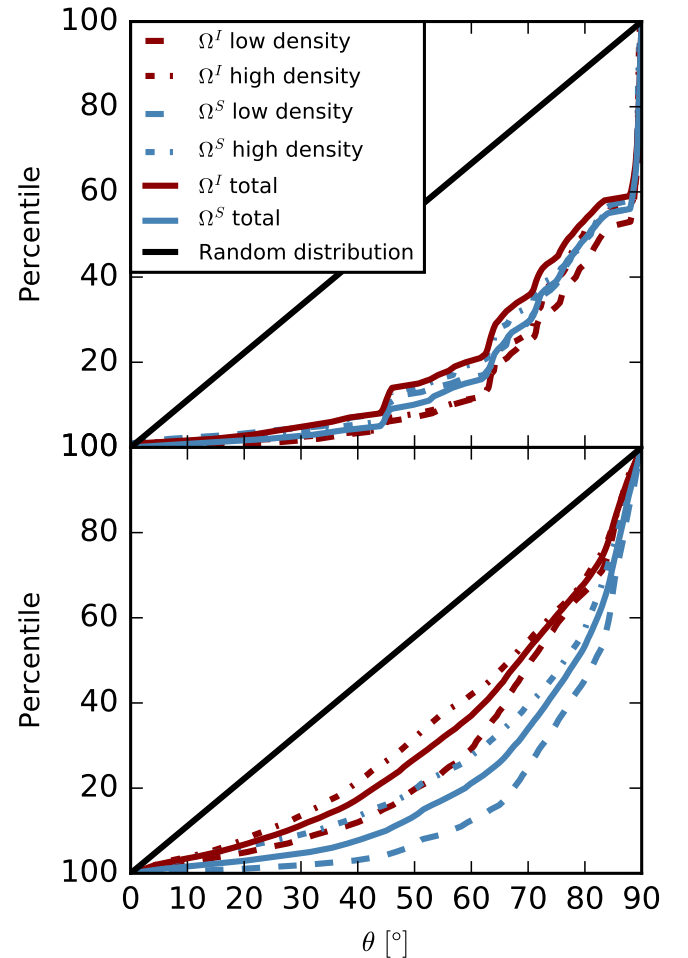


FIG. 8.— Cumulative pseudo-angle distribution for the case of $B = 10$ *top panel* and $B = 1$ *bottom panel*. In *dark red* the gradient for the intensity and in *blue* the gradient for the un-normalized centroid for all densities. Straight lines correspond to the gradient for all column density, dash lines for low column density and dot-dash for high column density.

TABLE 4
COLUMN DENSITY EFFECTS

		Model B = 10		Model B = 1	
		σ	m	σ	m
Ω^I	low	20°	83°	32°	71°
	high	21°	80°	38°	67°
Ω^S	low	25°	81°	20°	82°
	high	25°	81°	32°	76°

6.3. Comparison with other techniques

As we discussed, other techniques to study magnetic fields have their own limitations. For instance, the measurements of polarization arising from aligned dust are done in the optical/near-IR for stars and far-IR/sub-mm for dust. The interpretation of these measurements requires an understanding of the dust alignment and modeling its failure for high optical depths. In spite of the significant progress of the grain alignment theory (see Lazarian & Hoang 2007, 2008; Hoang & Lazarian 2008, 2009, 2016) the dust polarimetric studies of magnetic fields face difficulties related to the necessity of detailed modeling of the radiation field. If the radiative field is insufficient the grain alignment fails and does not reveal magnetic fields (see review by Andersson et al. 2015). Therefore, our suggestion to trace magnetic fields using velocity gradients has its advantages compared to the traditional technique that uses dust polarization. Note that no polarimetry is required for our technique. Furthermore, the classical C-F method requires polarization and spectroscopic velocity measurements to determine the intensity of the magnetic field. The polarization measurements require an understanding of dust alignment – currently under study. Our modified C-F analysis only requires the velocity measurements. With those, both the angle dispersion, with the velocity gradient and the velocity dispersion are estimated, giving the intensity of the magnetic field. Furthermore, our technique does not require highly sensitive data as the Zeeman effect and the Goldreich-Kylafis effect.

The direction of magnetic fields can also be obtained using statistical techniques that use the predicted Goldreich & Sridhar (1995) anisotropies of MHD turbulence (Lazarian et al. 2002; Esquivel & Lazarian 2005). Those techniques were used and showed that the magnetic fields obtained with them are in agreement with the measurements using dust polarization (Heyer et al. 2008). However, being statistical in nature, the techniques fail to provide point-wise magnetic-field directions. In comparison, the suggested technique provides a more detailed tracing of the magnetic field. We also showed in this paper that the velocity centroid gradients trace magnetic fields better than the gradients of densities.

In general, we believe that the synergy of different techniques is the best for tracing magnetic fields and the proposed technique can be useful for studying magnetic fields in diffuse ISM and molecular clouds.

6.4. Interferometric studies using velocity gradients

Gradients can be measured using interferometers and their advantage is that it is not necessary to restore the images first. For instance in Gaensler et al. (2011) and Burkhart et al. (2012) polarization gradients were used

for studying turbulence for the data with single dish observations missing.

The velocity centroids can be calculated using raw interferometric data (see Kandel et al. 2016b). Therefore gradients can be obtained with this data and be used to trace magnetic fields in distant objects, e.g. in other galaxies. We are going to present the examples of the corresponding studies elsewhere.

7. CONCLUSIONS

This work presents a new method, the Velocity Gradient Technique (VGT), of estimating the direction and magnitude of the projected magnetic field by means of the velocity gradient, Ω , requiring only spectroscopic data. Hence no polarization measurements nor dust alignment models are necessary. The method is based on the fact that the eddies align with the local 3D magnetic field, and that the eddies have a velocity gradient outwards. To test the method we use synthetic observations constructed with 3D MHD simulations. Further analysis with a wider set of initial conditions should be explored to fully understand the implications and limitations of the technique. A summary of the work and our major conclusions is as follows:

1.- Velocity Gradients (VGs) Ω that are available with velocity centroids can be used to estimate the direction of the mean magnetic field in a sub- and trans-Alfvénic regime.

2.- Using VGs we proposed a technique similar to the Chandrasekhar-Fermi one for determining the level of magnetization of the media given by the Alfvén Mach number M_A and the magnetic field intensity. This new technique only requires spectroscopic velocity data. Our numerical testing showed that the suggested expressions can provide a reliable way to estimate magnetic field strength.

3.- The degree of anisotropy of VG distribution depends on media magnetization. Hence, a measurement of its correlation function is another way of using VG for magnetic field studies. Moreover, by measuring the L-moments (statistical moments) of the velocity gradient we can determine the direction and strength of the magnetic field.

4.- The velocity gradient technique was applied to data with different levels of magnetization. It was then filtered depending on the column density measurements into three (low, mid and high). The regions with low column density data minimize error estimates for the direction of the magnetic field, while high column density does the opposite.

5.- VG tracing of magnetic fields improves when the regions of high density are excluded. In practical studies this means the regions of high column densities should be excluded. Our numerical study indeed showed that the regions with low column density data minimize error estimates for the direction of the magnetic field.

6.- We showed that the VG can work in the presence of averaging arising from finite telescope resolution. The accuracy of tracing, naturally, decreases with the decrease of the telescope resolution.

We thank Jungyeon Cho and Grzegorz Kowal for the data cubes and insightful discussions, and Julie

Davis and Dhanesh Krishnarao for insightful discussions. AL and DFGC are supported by the NSF grant AST 1212096. Partial support for DFGC was provided by CONACyT (Mexico). AL acknowledges a distinguished

visitor PVE/CAPES appointment at the Physics Graduate Program of the Federal University of Rio Grande do Norte and thanks the INCT INEspao and Physics Graduate Program/UFRN, at Natal, for hospitality.

REFERENCES

- Andersson, B.-G., Lazarian, A., and Vaillancourt, J. E. 2015, *ARA&A*, 53, 501 [6.3](#)
- Armstrong, J. W., Rickett, B. J., and Spangler, S. R. 1995, *ApJ*, 443, 209 [1](#)
- Beresnyak, A., Lazarian, A., and Cho, J. 2005, *ApJ*, 624, L93 [3](#), [4.1](#), [4.3](#)
- Burkhart, B., Collins, D. C., and Lazarian, A. 2015, *ApJ*, 808, 48 [1](#)
- Burkhart, B., Falceta-Gonçalves, D., Kowal, G., and Lazarian, A. 2009, *ApJ*, 693, 250 [2](#), [3](#)
- Burkhart, B., Lazarian, A., and Gaensler, B. M. 2012, *ApJ*, 749, 145 [6.4](#)
- Burkhart, B. et al. 2014, *ApJ*, 790, 130 [2](#), [4.1](#), [4.2](#)
- Chandrasekhar, S. and Fermi, E. 1953, *ApJ*, 118, 113 [1](#)
- Chepurnov, A., Burkhart, B., Lazarian, A., and Stanimirovic, S. 2015, *ApJ*, 810, 33 [1](#)
- Chepurnov, A. and Lazarian, A. 2010, *ApJ*, 710, 853 [1](#)
- Chepurnov, A. et al. 2010, *ApJ*, 714, 1398 [1](#)
- Cho, J. and Lazarian, A. 2002a, *Physical Review Letters*, 88, 245001 [2](#)
- . 2002b, *Physical Review Letters*, 88, 245001 [3](#)
- Cho, J., Lazarian, A., and Vishniac, E. T. 2002a, *ApJ*, 566, L49 [1](#)
- . 2002b, *ApJ*, 564, 291 [2](#)
- Cho, J. and Vishniac, E. T. 2000, *ApJ*, 539, 273 [2](#)
- Cho, J. and Yoo, H. 2016, *ApJ*, 821, 21 [1](#)
- Clark, S. E., Peek, J. E. G., and Putman, M. E. 2014, *ApJ*, 789, 82 [6.2](#)
- Crutcher, R. M. 2012, *ARA&A*, 50, 29 [1](#)
- de Avillez, M. A. and Breitschwerdt, D. 2005, *A&A*, 436, 585 [1](#)
- Draine, B. T. 2011, *Physics of the Interstellar and Intergalactic Medium* (Princeton University Press) [1](#)
- Draine, B. T. and Lazarian, A. 1998, *ApJ*, 494, L19 [3](#)
- Elmegreen, B. G. and Scalo, J. 2004, *ARA&A*, 42, 211 [1](#)
- Esquivel, A. and Lazarian, A. 2005, *ApJ*, 631, 320 [1](#), [2](#), [4.1](#), [4.2](#), [5.2](#), [6.3](#)
- Esquivel, A. and Lazarian, A. 2009, in *Revista Mexicana de Astronomía y Astrofísica Conference Series*, Vol. 36, *Revista Mexicana de Astronomía y Astrofísica Conference Series*, 45–53 [1](#), [4.1](#)
- Esquivel, A., Lazarian, A., and Pogossyan, D. 2015, *ApJ*, 814, 77 [2](#), [4.2](#)
- Esquivel, A., Lazarian, A., Pogossyan, D., and Cho, J. 2003, *MNRAS*, 342, 325 [5.2](#)
- Evans, II, N. J. 1999, *ARA&A*, 37, 311 [6.2](#)
- Falceta-Gonçalves, D., Lazarian, A., and Kowal, G. 2008, *ApJ*, 679, 537 [1](#)
- Falgarone, E., Troland, T. H., Crutcher, R. M., and Paubert, G. 2008, *A&A*, 487, 247 [1](#)
- Federrath, C. et al. 2010, *A&A*, 512, A81 [2](#)
- Ferrière, K. M. 2001, *Reviews of Modern Physics*, 73, 1031 [1](#)
- Gaensler, B. M. et al. 2011, *Nature*, 478, 214 [6.4](#)
- Goldreich, P. and Sridhar, S. 1995, *ApJ*, 438, 763 [1](#), [2](#), [2](#), [6.3](#)
- Heyer, M., Gong, H., Ostriker, E., and Brunt, C. 2008, *ApJ*, 680, 420 [2](#), [6.3](#)
- Heyer, M. H. and Brunt, C. M. 2004, *ApJ*, 615, L45 [1](#)
- Higdon, J. C. 1984, *ApJ*, 285, 109 [2](#)
- Hoang, T. and Lazarian, A. 2008, *MNRAS*, 388, 117 [6.3](#)
- . 2009, *ApJ*, 697, 1316 [6.3](#)
- . 2016, *ArXiv e-prints* [6.3](#)
- Hosking, J. R. M. 1990, *Journal of the Royal Statistical Society. Series B (Methodological)*, 52, 105 [5.3](#)
- Houde, M. et al. 2009, *ApJ*, 706, 1504 [1](#)
- Kandel, D., Lazarian, A., and Pogossyan, D. 2016a, *MNRAS*, 461, 1227 [2](#), [4.1](#), [2](#)
- . 2016b, *ArXiv e-prints* [2](#), [6.4](#)
- Kleiner, S. C. and Dickman, R. L. 1985, *ApJ*, 295, 466 [4.1](#)
- Koch, E. W. and Rosolowsky, E. W. 2015, *MNRAS*, 452, 3435 [6.2](#)
- Kowal, G. and Lazarian, A. 2010, *ApJ*, 720, 742 [2](#)
- Kowal, G., Lazarian, A., and Beresnyak, A. 2007, *ApJ*, 658, 423 [2](#), [3](#), [3](#), [4.1](#)
- Kowal, G., Lazarian, A., Vishniac, E. T., and Otmianowska-Mazur, K. 2009, *ApJ*, 700, 63 [3](#)
- Lazarian, A. 2007, *J. Quant. Spec. Radiat. Transf.*, 106, 225 [1](#)
- Lazarian, A., Andersson, B.-G., and Hoang, T. 2015, *Grain alignment: Role of radiative torques and paramagnetic relaxation*, 81 [1](#)
- Lazarian, A. et al. 2009, *Space Sci. Rev.*, 143, 387 [1](#)
- Lazarian, A. and Hoang, T. 2007, *MNRAS*, 378, 910 [6.3](#)
- . 2008, *ApJ*, 676, L25 [6.3](#)
- Lazarian, A. and Pogossyan, D. 2000, *ApJ*, 537, 720 [1](#), [2](#), [4.1](#)
- . 2004, *ApJ*, 616, 943 [4.1](#)
- . 2008, *ApJ*, 686, 350 [4.1](#)
- Lazarian, A., Pogossyan, D., and Esquivel, A. 2002, in *Astronomical Society of the Pacific Conference Series*, Vol. 276, *Seeing Through the Dust: The Detection of HI and the Exploration of the ISM in Galaxies*, ed. A. R. Taylor, T. L. Landecker, & A. G. Willis, 182 [1](#), [6.3](#)
- Lazarian, A. and Vishniac, E. T. 1999, *ApJ*, 517, 700 [2](#), [2](#)
- Lazarian, A. et al. 2012, *Space Sci. Rev.*, 173, 557 [2](#)
- Maron, J. and Goldreich, P. 2001, *ApJ*, 554, 1175 [2](#)
- McKee, C. F. and Ostriker, E. C. 2007, *ARA&A*, 45, 565 [1](#)
- Miesch, M. S., Scalo, J., and Bally, J. 1999, *ApJ*, 524, 895 [1](#), [4.1](#)
- Miville-Deschênes, M.-A., Levrier, F., and Falgarone, E. 2003, *ApJ*, 593, 831 [1](#)
- Montgomery, D. and Turner, L. 1981, *Physics of Fluids*, 24, 825 [2](#)
- Münch, G. and Wheelon, A. D. 1958, *Physics of Fluids*, 1, 462 [4.1](#)
- Novak, G., Dotson, J. L., and Li, H. 2009, *ApJ*, 695, 1362 [1](#)
- Ntormousi, E., Hennebelle, P., André, P., and Masson, J. 2016, *A&A*, 589, A24 [6.2](#)
- O’deil, C. R. and Castaneda, H. O. 1987, *ApJ*, 317, 686 [4.1](#)
- Ostriker, E. C. 2003, in *Lecture Notes in Physics*, Berlin Springer Verlag, Vol. 614, *Turbulence and Magnetic Fields in Astrophysics*, ed. E. Falgarone & T. Passot, 252–270 [1](#)
- Ostriker, E. C., Stone, J. M., and Gammie, C. F. 2001, *ApJ*, 546, 980 [1](#)
- Padoan, P. et al. 2001, *ApJ*, 559, 1005 [1](#)
- Padoan, P., Juvela, M., Kritsuk, A., and Norman, M. L. 2009, *ApJ*, 707, L153 [1](#)
- Planck Collaboration et al. 2016, *A&A*, 586, A135 [6.2](#)
- Shebalin, J. V., Matthaeus, W. H., and Montgomery, D. 1983, *Journal of Plasma Physics*, 29, 525 [2](#)
- Soler, J. D. et al. 2013, *ApJ*, 774, 128 [4.3](#), [3](#)
- Stanimirović, S. and Lazarian, A. 2001, *ApJ*, 551, L53 [1](#)
- Wang, Q. J. 1996, *Water Resources Research*, 32, 3617 [5.3](#)
- Xu, S., Lazarian, A., and Yan, H. 2015, *ApJ*, 810, 44 [1](#)
- Yan, H. and Lazarian, A. 2012, *J. Quant. Spec. Radiat. Transf.*, 113, 1409 [1](#)
- Zwillinger, D. and Kokoska, S. 1999, *Standard probability and Statistics tables and formulae* (Chapman & Hall/CRC) [4.2](#)